Gating of Heteromeric Retinal Rod Channels by Cyclic AMP: Role of the C-Terminal and Pore Domains

Nelly Bennett, Michèle Ildefonse, Frédérique Pagès, and Michel Ragno
Département de Biologie Moléculaire et Structurale, Laboratoire BMC (UMR CNRS 5090), CEA-Grenoble, Grenoble, France

ABSTRACT Cyclic nucleotide-gated channels are tetramers composed of homologous α and β subunits. C-terminal truncation mutants of the α and β subunits of the retinal rod channel were expressed in *Xenopus* oocytes, and analyzed for cGMP- and cAMP-induced currents (single-channel records and macroscopic currents). When the α subunit truncated downstream of the cGMP-binding site (αD608stop) is co-injected with truncated β subunits, the heteromeric channels present a drastic increase of cAMP sensitivity. A partial effect is observed with heteromeric αR656stop-containing channels, while αK665stop-containing channels behave like $\alpha wt/\beta wt$. The three truncated α subunits have wild-type activity when expressed alone. Heteromeric channels composed of αwt or truncated α subunits and chimeric β subunits containing the pore domain of the α subunit have the same cAMP sensitivity as α-only channels. The results disclose the key role of two domains distinct from the nucleotide binding site in the gating of heteromeric channels by cAMP: the pore of the β subunit, which has an activating effect, and a conserved domain situated downstream of the cGMP-binding site in the α subunit (I609-K665), which inhibits this effect.

INTRODUCTION

The cyclic GMP-activated rod channels, situated in the plasma membrane of retinal rod outer segments, are responsible for the entry of cations (mainly sodium, but also calcium) in the cell in the dark. Upon light-induced activation of the phototransduction cascade the concentration of cGMP is reduced, which results in closure of the channels and hyperpolarization of the cell. The retinal rod channel belongs to the family of cyclic nucleotide-gated (CNG) channels, involved in sensory transduction, which are activated by direct binding of the cyclic nucleotide to a site situated in the cytoplasmic C-terminal region. The three types of CNG channels (rod, olfactory neuron, and cone channels) are tetramers (for a review see Zagotta and Siegelbaum, 1996) composed of at least two (rod, cone) or three (olfactory neuron) types of homologous subunits (Chen et al., 1993; Körschen et al., 1995; Biel et al., 1996; Sundin et al., 2000; Kohl et al., 2000; Gerstner et al., 2000; Liman and Buck, 1994; Bradley et al., 1994; Sautter et al., 1998; Bönigk et al., 1999). Only the α subunits can form functional channels when expressed alone; β subunits have no channel activity on their own, but when co-expressed with α subunits, modify several characteristics of the channels, among which is the sensitivity to cAMP. The sensitivity to cAMP of heteromeric rod channels expressed in oocytes is higher than that of α-only channels (Fodor and Zagotta, 1996; Gordon et al., 1996; Shammat and Gordon, 1999; Pagès et al., 2000), and similar to that of native channels (Tanaka et al., 1989; Gavazzo et al., 1996; Picco et al., 1996). The rod heteromeric channel is also much more sensitive to L-*cis*-diltiazem (Chen et al., 1993; Körschen et al., 1995) than the homomeric channel. This property can be used to check that the two subunits indeed associate, or to estimate the homogeneity of the channel population obtained when co-injecting α and β mRNAs.

The structure of the nucleotide binding site of the rod α subunit was predicted by homology with the cAMP binding site of the catabolite gene activator protein (CAP) of *Escherichia coli* (Kumar and Weber, 1992), which is also homologous to that of the regulatory subunits of the cAMP- and cGMP-activated protein kinases (Kaupp et al., 1989; Shabb and Corbin, 1992): it consists of an α-helix (A), followed by eight β-rolls, and two additional α-helices (B and C). In CAP, binding of cAMP modifies the orientation of the DNA binding domain situated downstream of the cAMP binding site (Passner et al., 2000), while in the regulatory subunits of cAMP/cGMP dependent kinases, the effector domain is situated upstream of the nucleotide binding site, revealing some variability in cyclic nucleotide-induced activation. Binding of the nucleotide to the nucleotide binding site in CNG channels induces an allosteric transition that allows the channel to open, and cations to pass through the pore formed by the assembled pore-domains of the four subunits. The pore is homologous to that of voltage-gated K^+ channels except at the level of the selectivity filter, where it is shorter. Structure predictions of the pore domain of the rod channel, based on the structure of the KcsA K^+ channel (Doyle et al., 1998; Perozo et al., 1999) have allowed great progress in the approach of the gating mechanism. The pore of the α subunit was shown to undergo a conformation change associated with channel opening (Becchetti et al., 1999; Becchetti and Roncaglia, 2000; Liu and Siegelbaum, 2000). Recently, it was proposed that rotation of the domain situated between the last transmembrane helix (S6, downstream of the pore domain) and the nucleotide-binding site ("C-linker") initiates rota-

Submitted February 6, 2002, and accepted for publication April 5, 2002.
Address reprint requests to Dr. Nelly Bennett, BBSI/DBMS, CEA-Grenoble, 17 rue des Martyrs, 38054 Grenoble Cedex 9, France. Tel.: 33-4-38-78-33-95; Fax: 33-4-38-78-61-07/44-99; E-mail: nbennett@cea.fr.

0006-3495/02/08/920/12 $2.00

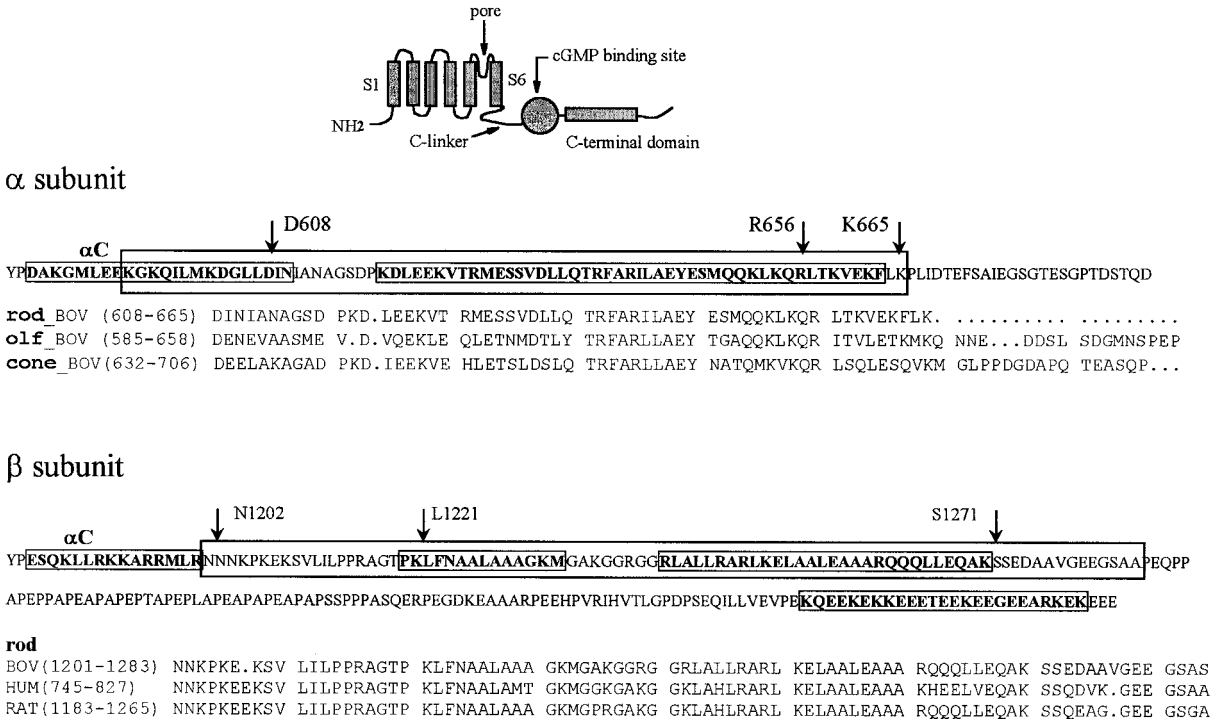

FIGURE 1 C-terminal domains of the rod channel α and β subunits. A ProDom NCBI-BLASTP2 search was performed for the C-terminal domains downstream of the cGMP-binding site of the bovine rod α (609–690) (CNG1 bovin) and β (1202–1394) (CNG4 bovin) subunits (ProDom server, Corpet et al., 2000. Two conserved domains were found: PD004548 for the α subunit (26 sequences, including rod, olfactory neuron and cone α subunits from mammals, chick rod and cone α subunits, and CNG channel from catfish, Drosophila, and *C. elegans*), and PD012882 for the β subunit (6 sequences, corresponding to all known rod β subunits). The sequences corresponding to these domains are boxed on the sequence of the C-terminus of the bovine rod α (CNG1) and β (CNG4c, Biel et al., 1996) subunits. The residues that are predicted to form an α-helix (The PredictProtein server for protein structure prediction, Rost and Sander, 1993) are in bold letters and boxed. The sites of truncations are indicated by arrows. The nucleotide binding site ends at the C-terminal end of the αC helix. The scheme represents the common secondary structure of α and β subunits. Alignments of several sequences corresponding to the part of PD004548 and PD012882 domains situated downstream of the nucleotide binding site are shown below each sequence. The sequence of the bovine rod β subunit in the alignment is that of Körschen et al., 1995.

tion of S6 and pore opening (Johnson and Zagotta, 2001; Flynn and Zagotta, 2001).

A segment of ~50 residues, situated immediately downstream of the C-helix of the binding site in the rod channel α subunits (I611-K665), is highly conserved among rod, olfactory neuron, and cone channels (Fig. 1). This domain was classified as "PD004548" in the ProDom release 2000.1 (Corpet et al., 2000) when this work started. In the ProDom release 2001.2, PD004548 also includes part of the last helix (αC) of the nucleotide binding site. A conserved domain (PD012882) is present in a similar position downstream of the nucleotide binding site of all known (bovine, human, rat) rod β subunits (1202–1282 in the bovine rod β subunit); this domain is not conserved in other β subunits, but the second olfactory β subunit (Sautter et al., 1998: CNG4.3; Bönigk et al., 1999: CNGβ1b), which associates with the other olfactory OCNC1 and OCNC2 subunits to form the olfactory neuron channel, is identical to the rod β subunit. This suggests that the domains downstream of the cGMP-binding site may be important for channel assembly or function. According to PHD (Profile network prediction HeiDelberg) structure prediction (Rost and Sander, 1993) (Fig. 1), PD004548 (α subunit) downstream of the cGMP-binding site consists for the most part of an α-helix (K619-F663), which is predicted by the program COILS (Lupas, 1996) as having a high probability of forming a coiled-coil domain (not shown). The PD012882 domain in the β subunit also presents a predicted α-helical structure composed of two helices (P1219-M1232 and R1241-K1270); the second α-helix is also susceptible to form a coiled-coil domain, although with a lesser probability than the α-helix in PD004548.

The pore domains of all CNG channel α subunits are highly homologous, and all lack the YG residues in the GYGD sequence which is characteristic of the K^+ channel selectivity filter. The pore domain of β subunits from rod and cone channels is homologous to that of α subunits, but has different charged residues. An alignment is shown in Fig. 2.

We took advantage of the different properties of homomeric and heteromeric channels concerning the sensitivity to cAMP to investigate the possible role of the conserved C-terminal domains of the α and β subunits, which has not been studied previously. We report here a study of several C-terminal truncations of the α subunit, expressed alone or

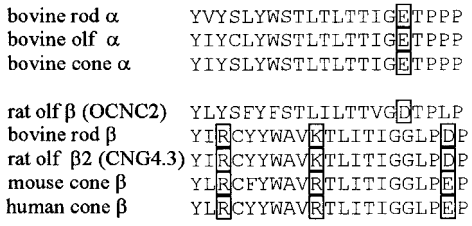

FIGURE 2 Alignment of the pore domains of rod, olfactory neuron (olf), and cone α and β subunits. Conserved charged residues are boxed.

co-expressed with β subunits, wild type, or truncated in their C-terminal domain. We also studied possible functional differences conferred by the pore of the β subunit by constructing chimeras of the two rod subunits with exchanged pore domains.

MATERIALS AND METHODS

cDNAs and mutations

The bovine rod α subunits were a gift of Prof. U. B. Kaupp. The bovine rod β subunit CNG4c (Biel et al., 1996) starting at V572 downstream of the GARP region previously described (Pagès et al., 2000) was used. Residue numbers in the β subunit correspond to the sequence of the complete β subunit (Körschen et al., 1995). The α and β subunits are inserted in the pGemHe vector (Liman et al., 1992), and the ATG codon is preceded by a Kozak consensus sequence (CCACC) (Kozak, 1984). Truncations were constructed by PCR by introducing a stop codon at the required position.

Construction of the β[α-pore] chimera

A fragment of the β subunit containing the pore was subcloned into pBluescript. *Eco*RI and *Bam*HI restriction sites were introduced by silent mutations at the 5′ and 3′ ends of the pore domain: ggG AAT TCt (*Eco*RI) in 5′ at the position corresponding to $G_{933}N_{944}S_{945}$, and ccG GAT CCt (*Bam*H1) in 3′ at the position corresponding to $P_{964}D_{965}P_{966}$. The two complementary oligonucleotides corresponding to the complete pore domain of the α subunit with the *Eco*R1 and *Bam*H1 restriction sites at the 5′ and 3′ ends were synthesized and ligated in place of the pore domain in the β subunit fragment. The fragment containing the pore of the α subunit was then exchanged for the corresponding fragment in the wild-type β subunit, giving the β[α-pore] construct (corresponding mutated protein domain: $N_{944}S$*YVYSLYWSTLTLTTIGET*PDP_{966}).

Construction of the α[β-pore] chimera

A fragment of the α subunit containing the pore was subcloned into pBluescript. The *Eco*R1 and *Bam*H1 sites were introduced at the 5′ and 3′ ends of pore domain of the α subunit cDNA, mutating the $A_{344}R_{345}K_{346}$ sequence upstream of the pore into ANS (GCG AAT TCA), and the last three residues of the pore ($P_{365}P_{366}P_{367}$) into PDP (ccG GAT CCt). The pore domain of the β subunit with the *Eco*R1/*Bam*H1 restriction sites was excised from the mutated β construct (containing the two restriction sites) in pBluescript, and ligated in place of the pore of the α subunit. A wild-type fragment containing the pore in the complete α*wt* cDNA in pGemHe was then exchanged for the corresponding fragment containing the pore of the β subunit, giving the α[β-pore] construct (corresponding protein domain: N_{345}*SYIRCYYWAVKTLITIGGLPDP*$_{367}$). All mutations were verified by sequencing.

Channel expression

Capped mRNAs were synthesized in vitro from linearized plasmids in the presence of RNA cap structure analogs (New England Biolabs, Beverly, MA), and injected into *Xenopus* oocytes (25 ng/oocyte for macroscopic currents or 0.25 ng/oocyte for single-channel records). For coexpression of α and β subunits, β mRNA and α mRNA were mixed and injected into the oocyte. The β/α ratio was between 2 and 3. Oocytes were incubated in Barth's medium for 2–10 days at 19°C for macroscopic currents (or at 4°C after 18–24 h at 19°C for single-channel currents) before measurements.

Patch-clamp recording of excised inside-out patches

The solution in the pipette and in the perfusion medium was 100 mM KCl, 10 mM EGTA/KOH, 10 mM Hepes/KOH, pH 7.2. The cytoplasmic face of the patch was superfused by solutions containing variable nucleotide concentrations using an RSC100 rapid solution changer (Bio-Logic, Claix, France). The saturating cGMP and cAMP concentrations were, respectively, 500 μM and 20 mM. Currents were recorded with an RK-400 patch amplifier (Bio-Logic).

P_{omax} (open probability at saturating concentrations of cGMP and cAMP) was obtained from single-channel record analysis. Single-channel records at +80 mV (20–30-s duration) sampled at 33 kHz and numerically filtered (Hanning window) at 1 kHz were used to compute amplitude histograms using the Bio-Patch software (Bio-Logic). The same current interval (4 pA) for all records was divided into 50 classes for building the histograms. The maximum number of events/pA was at least 10^6. The histograms were fitted with two or three Gaussian curves. Similar P_{omax} values were obtained from records filtered at 4 kHz, as previously described (Pagès et al., 2000).

Macroscopic currents induced by voltage steps (500 ms, ±80 mV) were low-pass filtered at 300 Hz and digitized at 1 kHz using pCLAMP 6.0 (Axon Instruments, Union City, CA). The series resistance was compensated for (resulting value <1 MΩ). Each record was averaged three times. Dose-response curves were obtained by plotting the current at +80 mV as a function of nucleotide concentration after subtraction of the leak current.

Curve fitting

Data were fitted with the Hill equation or the Monod-Wyman-Changeux (MWC) model (Monod et al., 1965) using the Microcal Origin software.

Hill equation

$I/I_{max} = 1/(1 + (EC_{50}/X)^{nH})$, with EC_{50} the ligand concentration that gives half-maximal effect, n_H the Hill number, and X the ligand concentration.

MWC model

Assuming that the rod channel is a tetramer (Liu et al., 1996), the proportion of channels in the R (open) state is given by $\bar{R} = (1 + X/K_R)^4/((1 + X/K_R)^4 + L(1 + cX/K_R)^4)$, in which X is the ligand concentration, $L = [T]/[R]$, T corresponds to the closed state, and $c = K_R/K_T$ (dissociation constants of the ligand for the R and T states).

Chemicals

L-*cis*-Diltiazem was a gift of Synthelabo Recherche (Bagneux, France).

RESULTS

Role of the C-terminal domains

To determine whether the C-terminal domains downstream of the nucleotide binding site may be involved in channel gating, we studied the effect of C-terminal truncations on the efficacy of cAMP and cGMP. The sites of truncation were chosen according to the predicted structure of the C-terminal domains (Fig. 1). The α subunit was truncated after K665 (the last residue of the conserved PD004548 domain), R656 (deleting part of PD004548), and D608 (deleting the whole C-terminal domain downstream of the nucleotide binding site, including the last two residues of the αC-helix). The β subunit was truncated after S1271 (at the end of the predicted helical domain of PD012882), L1221 (the third residue of the first predicted α helix of PD012882 downstream of the nucleotide binding site), and N1202 (deleting the whole C-terminal domain downstream of the nucleotide binding site). Like the βwt subunit, the truncated β subunits did not give rise to channel activity when expressed alone. The selectivity for cGMP versus cAMP was determined from single-channel records (from the open probability at saturating cGMP and cAMP concentrations) and from macroscopic currents ($I_{max(cAMP)}/I_{max(cGMP)}$ ratios) to obtain sufficient data for statistical analysis. When measuring macroscopic currents, the extent of inhibition by L-*cis*-diltiazem was used as a tool to test the homogeneity of the channel population: since the effect of diltiazem on mutated channels is unknown, this was first determined from single-channel records. The EC_{50} of several constructions for cGMP and cAMP were determined from macroscopic currents. All measurements were performed on excised inside-out patches.

Single-channel records

The αwt subunit or the truncated α subunits (αK665stop, αR656stop, and αD608stop) were co-expressed with βwt or the truncated βL1221stop. Single-channel records were used to determine the open probability of the different heteromeric channels in the presence of saturating concentrations of cGMP (P_{omax} cGMP), cGMP + L-*cis*-diltiazem, and cAMP (P_{omax} cAMP). The unitary currents had either the characteristics of α-only channels or markedly different characteristics, which were therefore attributed to heteromers. As previously described for oocytes co-injected with αwt and βwt mRNAs (Pagès et al., 2000), no channels with intermediate characteristics were observed, suggesting a unique subunit stoichiometry. Previous studies indeed suggest that under the condition used, heteromers of $\alpha_2\beta_2$ stoichiometry are obtained (Shammat and Gordon, 1999; He et al., 2000). Examples of single- (or two-) channel records of cGMP- and cAMP-induced currents from oocytes expressing heteromeric channels are shown in Fig. 3, and mean values (when possible) are displayed in Table 1.

Records from control αwt and $\alpha wt/\beta wt$ channels are shown for comparison: direct measurement of P_{omax} cAMP has not as yet been reported, but the values are consistent with published $I_{max(cAMP)}/I_{max(cGMP)}$ ratios, and records in the presence of cGMP and cGMP + diltiazem are consistent with our previous results (Pagès et al., 2000).

For all the mutated channels tested, the P_{omax} cGMP is close to 1, as observed for $\alpha wt/\beta wt$ channels, suggesting that neither C-terminal domain plays a major role in cGMP-induced activity. This high P_{omax} value allows unambiguous determination of the number of channels in the patch. The sensitivity to cAMP is, however, clearly modified by truncating the α subunit: a remarkable increase in P_{omax} cAMP is observed for αD608stop-containing heteromeric channels, and also, to a lesser extent with the αR656stop subunit, while αK665stop-containing heteromeric channels are very similar to $\alpha wt/\beta wt$ channels. For the three truncated α subunits results obtained with βwt and βL1221stop are similar, although with an apparently higher sensitivity to cAMP for βL1221stop compared to βwt.

Inhibition by L-*cis*-diltiazem is close to 100% for αK665stop- and αR656stop-containing heteromers, but notably reduced for the heteromeric channels containing the shorter α subunit αD608stop, with values intermediate between that for αwt and that for $\alpha wt/\beta wt$.

Although no single-channel record was obtained for αD608stop/βwt, and only one or two measurements are given in Table 1 for αR656stop/βwt, αD608stop/βL1221stop, and αR656stop/βL1221stop, qualitatively similar results were obtained for each channel type from several patches in which two or more channels were present: the example of a two-channel record shown in Fig. 3 for αD608stop/βwt channels clearly reveals an increased sensitivity to cAMP and reduced sensitivity to diltiazem compared to $\alpha wt/\beta wt$ channels. For αR656stop- and αK665stop-containing heteromeric channels, ~100% inhibition by diltiazem was also measured in several patches with two or three channels.

It is important to note that the P_{omax} values obtained from single-channel analysis may slightly vary depending on the record, due to the irregular occurrence of long closed periods, which are particularly frequent and long in cAMP, but also present in cGMP. The absence, or the long duration, of closed periods within the records used for analysis may lead to overestimated or underestimated P_{omax} values. As we failed to obtain a sufficient number of patches with a single channel, these values should be considered as indicative.

Macroscopic current measurements

Activity of rod α subunits truncated in their C-terminal domain (homomeric channels). As a control, the activity of the truncated α-only channels was studied from macroscopic current analysis. The results show that currents from all the truncated α-only channels present $I_{max(cAMP)}/$

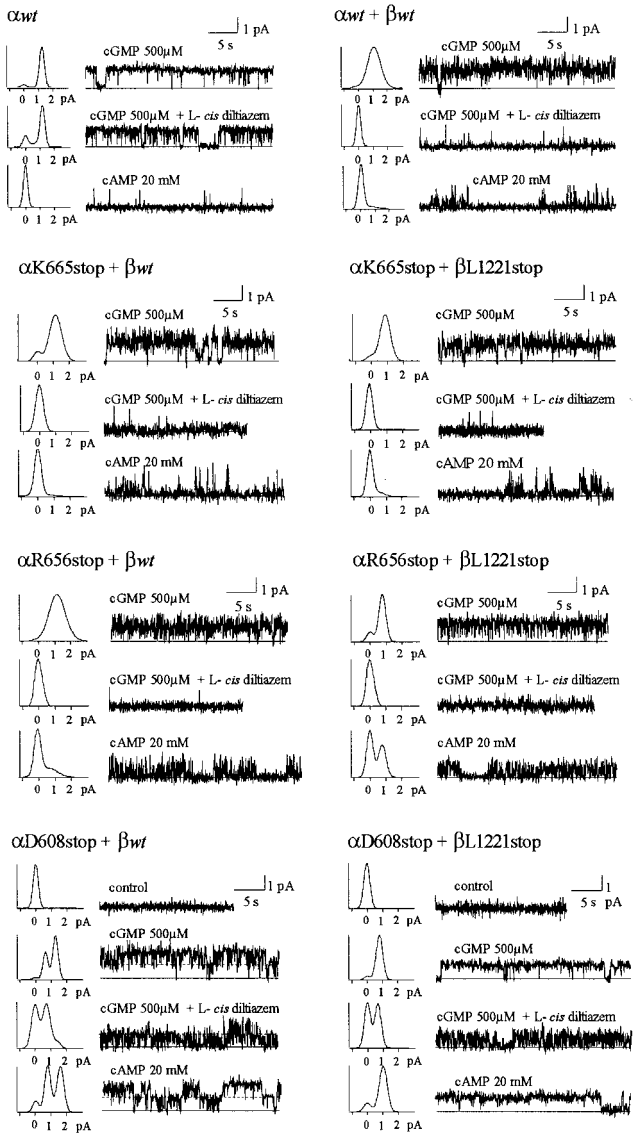

FIGURE 3 Examples of unitary cGMP and cAMP-induced currents for control wild-type channels and heteromeric channels with truncated α subunits (K665stop, R656stop, and D608stop) co-expressed with βwt or β L1221stop. cGMP: 500 μM; cAMP: 20 mM. P_{omax} values are obtained from the histograms computed from the whole length of the records shown. αwt: 0.93 (cGMP), 0.03 (cAMP); $\alpha wt + \beta wt$: 0.98 (cGMP), 0.12 (cAMP); αK665stop + βwt: 0.83 (cGMP), 0.11 (cAMP); αK665stop + βL1221stop: 0.94 (cGMP), 0.17 (cAMP); αR656stop + βwt: 0.99 (cGMP), 0.32 (cAMP); αR656stop + βL1221stop: 0.84 (cGMP), 0.45 (cAMP); αD608stop + βL1221stop: 0.93 (cGMP), 0.86 (cAMP). A two-channel record is shown for αD608stop + βwt (P_{omax} cGMP = 0.83, P_{omax} cAMP = 0.68): the high P_{omax} cAMP, with numerous simultaneous openings of two channels, unambiguously indicates that both channels are heteromers. Inhibition of the cGMP-induced current (500 μM cGMP) by L-*cis*-diltiazem (50 μM) is close to 100% for all channels, except αwt-only channels (11%), αD608stop/βwt (60%), and αD608stop/βL1221stop (46%). For calculation of P_{omax} in the patch with 2 channels (αD608stop/βwt), the following formula was used: $P_{omax} = 1 - \text{Sq. root}(1 - P_{o(measured)})$. Mean values of several experiments are given in Table 1. The activity of heteromeric channels with αK665stop and αR656stop subunits is more flickering than that of αwt channels, as previously described for $\alpha wt/\beta wt$ (Körschen et al., 1995). In the examples shown, the activity of heteromers containing the αD608stop subunit seems less flickering, and the amplitude of the cGMP- and cAMP-induced unitary currents appears smaller than that of wild-type channels (~1 pA compared to 1.35 pA).

$I_{max(cGMP)}$ ratios similar to those observed with αwt channels (Table 2). The EC_{50} for cGMP of αD608stop (33 $\pm$ 1 μM, see Fig. 6 below) is similar to that previously measured for αwt channels (29.9 $\pm$ 0.8 μM; Pagès et al., 2000), and inhibition by diltiazem is similar for the truncated and complete α subunits. Therefore, in the case of homomeric α channels, the whole domain downstream of D608 at the C-terminal end of the αC-helix of the nucleotide binding site can be deleted without a detectable effect on cGMP- and cAMP-induced currents.

Activity of heteromeric channels composed of wild-type or truncated α and β subunits. When measuring macroscopic currents from oocytes co-injected with the mRNAs of the two types of subunits, the homogeneity of the channel population in the patches was checked by comparing the selectivity for cGMP versus cAMP and the sensitivity to L-*cis*-diltiazem to those determined from unitary currents (Table 1).

The results obtained with truncated α subunits co-expressed with βwt subunits are indicated in Table 2. Consistent with the single-channel records, the $I_{max(cAMP)}/I_{max(cGMP)}$ ratio is similar to that of $\alpha wt/\beta wt$ channels when the βwt subunit is co-expressed with the truncated αK665stop, and significantly higher when it is co-expressed with the shorter αD608stop subunit. For αR656stop/βwt, however, the $I_{max(cAMP)}/I_{max(cGMP)}$ ratio is not significantly different from that measured for $\alpha wt/\beta wt$ channels, and both the $I_{max(cAMP)}/I_{max(cGMP)}$ ratio and inhibition by L-*cis*-diltiazem are notably lower than those measured from single-channel records. Although, as noted above, there might be some uncertainty in the P_{omax}(cAMP)/P_{omax}(cGMP) ratios in Table 1, the lower inhibition by diltiazem measured from macroscopic currents from oocytes co-injected with αR656stop and βwt mRNAs suggests that the patches contained a nonnegligible proportion of α-only channels. When measuring single-channel records from these oocytes and from oocytes co-injected with αD608stop and βwt mRNAs, channels with α-only characteristics were indeed observed. This suggests that for these two channel types, the $I_{max(cAMP)}/I_{max(cGMP)}$ ratios might be underestimated. The reason for this heterogeneity remains unclear.

In contrast, results from macroscopic currents obtained with heteromeric channels containing the truncated βL1221stop subunit ($I_{max(cAMP)}/I_{max(cGMP)}$ ratio and extent of inhibition by L-*cis*-diltiazem) are close to those obtained from single-channel records, suggesting that in these cases the channel populations mainly consisted of heteromeric channels. The increase of the $I_{max(cAMP)}/I_{max(cGMP)}$ ratio associated with increasing truncation of the α subunit is illustrated by examples of current records in Fig. 4, and mean

TABLE 1 Characteristics of unitary currents from wild-type rod channels (*αwt*, *αwt*/*βwt*), and heteromeric channels composed of truncated *α* subunits (*α*K665stop, *α*R656stop, or *α*D608stop) and *βwt* or *β*L1221stop

Injected mRNAs	P_{omax} cAMP	P_{omax} cGMP	$\frac{P_{omax}cAMP}{P_{omax}cGMP}$	Inhibition by Diltiazem (%)
αwt	0.02 ± 0.01 (9)	0.92 ± 0.04 (9)	0.022 ± 0.012	20 ± 3 (7)
αwt + *βwt*	0.18 ± 0.03 (7)	0.94 ± 0.01 (7)	0.19 ± 0.03	>97 (7)
αK665stop + *βwt*	0.10 ± 0.02 (6)	0.90 ± 0.03 (6)	0.11 ± 0.03	>97 (6)
αR656stop + *βwt*	0.32 (1)	0.99 (1)	0.32	>97 (1)
αK665stop + βL1221stop	0.19 ± 0.03 (4)	0.93 ± 0.02 (4)	0.20 ± 0.04	>97 (4)
αR656stop + βL1221stop	0.40 ± 0.05 (2)	0.89 ± 0.06 (2)	0.45 ± 0.08	>97 (2)
αD608stop + βL1221stop	0.86 (1)	0.93 (1)	0.92	46 (1)

The P_{omax} values were measured from amplitude histograms of single-channel records (cGMP, 500 μM; cAMP, 20 mM) of 20–30 s duration. The number of patches is indicated in parentheses, and the mean values are given ± SE. No single-channel record was obtained with αD608stop/*βwt*. Examples of currents are shown in Fig. 3.

values of several measurements are indicated in Table 2: as observed in single-channel records, truncation downstream of K665 has little or no effect, while the $I_{max(cAMP)}/I_{max(cGMP)}$ ratio is markedly increased for αR656stop/βL1221stop channels, and dramatically increased for αD608/βL1221stop channels. Qualitatively similar results were obtained with the two other truncated β subunits βS1271stop and βN1202stop. Dose-response curves for cGMP and cAMP measured with *αwt*/βL1221stop channels and αD608stop/βL1221stop channels are shown in Fig. 5. The EC_{50} of αD608stop/βL1221stop channels for cAMP (224 ± 6 μM) is dramatically reduced compared to that measured for an *αwt*/*βwt* or *αwt*/βL1221 channel; the EC_{50} for cGMP (22 ± 2 μM) is also reduced, to a lesser extent, compared to that of *αwt*/*βwt* channels or an *αwt*/βL1221 channel. The characteristics of *αwt*/βL1221stop channels ($I_{max(cAMP)}/I_{max(cGMP)}$ ratio, Table 2; EC50 for cGMP and cAMP, Fig. 5) are slightly different from those of *αwt*/*βwt* channels. Statistical analysis of the data suggests that the $I_{max(cAMP)}/I_{max(cGMP)}$ ratio measured with *αwt*/βL1221stop is significantly higher, and the EC_{50} for cGMP and cAMP significantly lower than those measured with *αwt*/*βwt* channels. Thus, truncating the C-terminal domain of the β subunit downstream of the nucleotide binding site may have a slight effect on cGMP and cAMP sensitivity, but this effect is much less dramatic than that of truncating the C-terminal domain of the α subunit. Both effects may add up in the double mutant, and account for the apparently higher cAMP sensitivity of αD608stop/βL1221stop compared to αD608stop/*βwt* channels (Table 2 and records in Fig. 3). The effects of truncating the C-terminal domains of α and β subunits on the EC_{50} for cGMP and cAMP and on the $I_{max(cAMP)}/I_{max(cGMP)}$ ratios are summarized in Fig. 6.

Density of functional channels at the plasma membrane. Macroscopic currents provide additional information that is

TABLE 2 Characteristics of macroscopic currents from rod homomeric *α* channels (*wt*, *α*K665stop, *α*R656stop, or *α*D608stop), and from heteromeric channels composed of *α* (*wt* or truncated) and *β* (*wt* or L1221stop) subunits

Injected mRNAs	$I_{max(cAMP)}/I_{max(cGMP)}$ (+80 mV)	Inhibition by Diltiazem (%)	$I_{max(cGMP)}$ (pA)
*αwt**	0.036 ± 0.005 (15)	15 ± 2 (6)	2505 ± 242 (15)
αK665stop	0.037 ± 0.004 (8)	21 ± 2 (7)	2340 ± 395 (8)
αR656stop	0.04 ± 0.01 (4)	–	3464 ± 882 (5)
αD608stop	0.021 ± 0.02 (12)	24 ± 2 (10)	3311 ± 39 (12)
αwt + *βwt**	0.15 ± 0.02 (11)	82 ± 3 (7)	2415 ± 300 (11)
αK665stop + *βwt*	0.18 ± 0.02 (9)	75 ± 4 (9)	1668 ± 661 (12)
αR656stop + *βwt*	0.22 ± 0.05 (21)	44 ± 3 (16)	2236 ± 589 (21)
αD608stop + *βwt*	0.26 ± 0.04 (15)	35 ± 3 (21)	166 ± 42 (35)†
αwt + βL1221stop	0.19 ± 0.01 (28)	92 ± 2 (6)	2460 ± 232 (28)
αK665stop + βL1221stop	0.18 ± 0.03 (16)	86 ± 4 (16)	3166 ± 997 (16)
αR656stop + βL1221stop	0.30 ± 0.03 (14)	85 ± 2 (13)	1350 ± 558 (14)
αD608stop + βL1221stop	0.82 ± 0.02 (25)	36 ± 3 (23)	222 ± 92 (26)†

The number of patches is indicated in parentheses, and the mean values are given ± SE. Inhibition by L-*cis*-diltiazem (50 μM) is measured at saturating cGMP concentration. Results for αR656stop + *βwt*, αD608stop + *βwt*, and αD608stop + βL1221stop are from two or three separate mRNA injections. Statistical analysis of the $I_{max(cAMP)}/I_{max(cGMP)}$ ratios: for *βwt*-containing heteromeric channels, only the sets of data measured with *αwt*/*βwt* and with αD608stop/*βwt* are significantly different at the 0.05 level; the data for αR656stop/βL1221stop and αD608stop/βL1221stop are significantly different from the data for *αwt*/βL1221stop, with $p = 5 \cdot 10^{-6}$ and $p < 10^{-40}$, respectively; the sets of data measured with *αwt*/βL1221stop and *αwt*/*βwt* are significantly different, with $p = 0.028$.

*$I_{max(cAMP)}/I_{max(cGMP)}$ from Pagès et al. (2000).

†The amplitude of the cGMP-induced current compared to that of control oocytes was 7% (αD608stop + *βwt*) and 4% (αD608stop + βL1221stop).

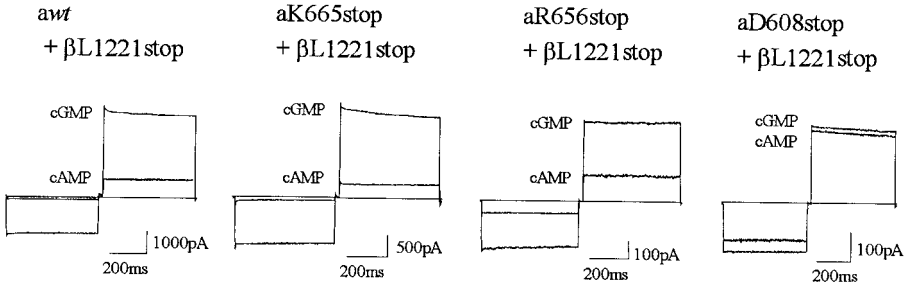

FIGURE 4 Examples of macroscopic cGMP and cAMP-induced currents illustrating the effect of C-terminal truncation of the α subunit on the cAMP sensitivity of heteromeric channels containing the βL1221stop subunit. cGMP: 500 μM; cAMP: 20 mM. The activity of the four channel types can be attributed for the most part to heteromeric channels by comparison of their sensitivity to L-*cis*-diltiazem and $I_{max(cAMP)}/I_{max(cGMP)}$ ratio to those of single channels. Mean values of several experiments are indicated in Table 2. The left part of each record is the current recorded at -80 mV, and the right part the current at $+80$ mV (see Methods).

not accessible from single-channel records: the amplitude of the currents, compared to that of control oocytes injected the same day with wild-type mRNAs, reflects the density of functional channels at the plasma membrane. While large currents of the same order as currents from control oocytes are observed with homomeric channels formed by each of the three truncated α subunits (Table 2) and with αK665stop- and αR656stop-containing heteromers, very small cGMP-induced currents are reproducibly measured when αD608stop mRNA is co-injected with βwt or

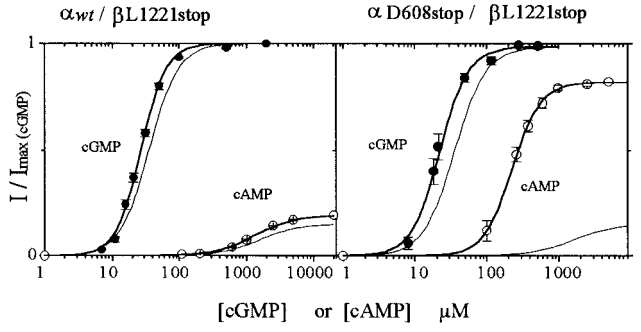

FIGURE 5 Dose-response curves for cGMP and cAMP-induced macroscopic currents from oocytes expressing heteromeric $\alpha wt/\beta$L1221stop and αD608stop/βL1221stop channels. The symbols represent the mean of different experiments, $\pm$SE. cGMP-induced currents are normalized to 1, and cAMP-induced currents to the $I_{max(cAMP)}/I_{max(cGMP)}$ ratio from Table 2. The fits of all the points to the Hill equation are shown on the graph. For $\alpha wt/\beta$L1221stop: EC_{50} cGMP = 27 $\pm$ 1 μM, n_H = 2.3 $\pm$ 0.1 (7 patches), and EC_{50} cAMP = 1353 $\pm$ 18 μM, n_H = 1.5 $\pm$ 0.1 (6 patches). For αD608stop/βL1221stop: EC_{50} cGMP = 22 $\pm$ 2 μM, n_H = 2.2 $\pm$ 0.2 (8 patches), and EC_{50} cAMP = 224 $\pm$ 6 μM, n_H = 2.2 $\pm$ 0.1 (8 patches). Hill fits of the dose-response curves for $\alpha wt/\beta wt$ (from Pagès et al., 2000) are indicated on both graphs with thin lines (EC_{50} cGMP: 35 $\pm$ 0.6 μM, n_H = 2 $\pm$ 0.1; EC_{50} cAMP: 1607 $\pm$ 31 μM, n_H = 1.45 $\pm$ 0.04). Note that the Hill number of the cAMP dose-response curve is lower than that of the cGMP dose-response curve for $\alpha wt/\beta wt$ and $\alpha wt/\beta$L1221stop channels, while the two n_H values are identical for the double mutant, consistent with the predictions of the MWC model according to which n_H increases with the gating efficacy of the ligand (Rubin and Changeux, 1966; see also Pagès et al., 2000). The sets of data for EC_{50} cGMP, EC_{50} cAMP, and $I_{max(cAMP)}/I_{max(cGMP)}$ measured from each experiment with $\alpha wt/\beta$L1221stop are significantly different from the corresponding sets of data measured with $\alpha wt/\beta wt$, with $p = 5.10^{-4}$, 0.006, and 0.028, respectively (independent *t*-test on two populations). The set of data for EC_{50} cGMP measured with αD608stop/βL1221stop is significantly different from that measured with $\alpha wt/\beta wt$ with $p = 7.10^{-5}$.

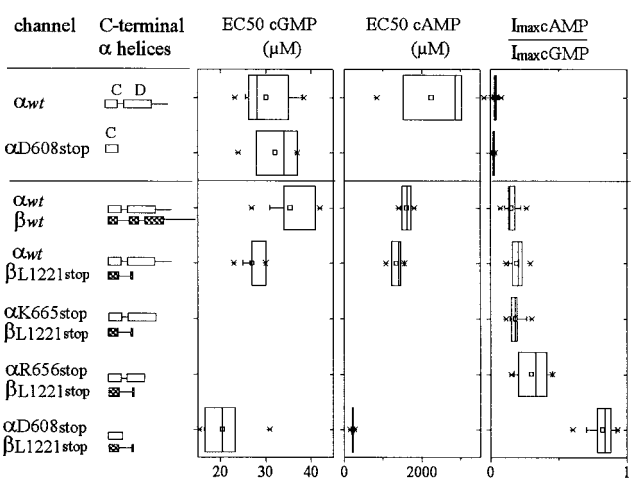

FIGURE 6 Summary of the effect of C-terminal truncations of α and β subunits on EC_{50} cGMP, EC_{50} cAMP, and $I_{max(cAMP)}/I_{max(cGMP)}$. Statistical box charts for EC_{50} (obtained by fitting each individual dose-response curve with the Hill equation) and $I_{max(cAMP)}/I_{max(cGMP)}$ ratios (obtained from I_{max} cAMP and I_{max} cGMP measured on the same patch), from macroscopic current measurements. Dose-response curves for cAMP were measured on patches that had very large cGMP-induced currents in the case of channel constructs with a low cAMP sensitivity (usually different patches were used for the two ligands). Data for αwt and $\alpha wt/\beta wt$ are from Pagès et al. (2000). The vertical lines in the box denote the 25th, 50th, and 75th percentile values. The error bars denote the 5th and 95th percentile values. The crosses are the extreme values, and the square in the box is the mean of the data. EC_{50} cGMP: 29.9 $\pm$ 08 μM, 8 patches (αwt); 33 $\pm$ 1 μM, 7 patches (αD608stop); 35 $\pm$ 0.6 μM, 11 patches (αwt + βwt); 27 $\pm$ 1 μM, 7 patches (αwt + βL1221stop); 22 $\pm$ 2 μM, 8 patches (αD608stop + βL1221stop). EC_{50} cAMP: 2077 $\pm$ 172, 8 patches (αwt); 1607 $\pm$ 31 μM, 9 patches (αwt + βwt); 1353 $\pm$ 18 μM, 6 patches (αwt + βL1221stop); 224 $\pm$ 6 μM, 8 patches (αD608stop + βL1221stop). For mean values of $I_{max(cAMP)}/I_{max(cGMP)}$ ratios, see Table 2.

TABLE 3 Characteristics of macroscopic currents from heteromeric rod channels with chimeric β subunits having an α-pore domain

Injected mRNAs	$I_{max(cAMP)}/I_{max(cGMP)}$ (+80 mV)	Inhibition by Diltiazem (%)	$I_{max(cGMP)}$ (pA)
αwt + β[α-pore]*	0.024 ± 0.002 (20)	67 ± 2 (20)	2826 ± 698 (20)
αR656stop + β[α-pore]L1221stop	0.023 ± 0.004 (11)	81 ± 2.5 (11)	740 ± 170 (11)
αD608stop + β[α-pore]L1221stop	0.03 ± 0.01 (2)	52 ± 9 (2)	30 ± 17 (16)

The number of patches is indicated in parentheses, and the mean values are given ± SE. Inhibition by L-*cis*-diltiazem is measured at saturating cGMP concentration. Note that the amplitude of currents of αD608stop/β[α-pore]L1221stop channels is low, as observed with αD608stop/βL1221stop channels. *Two separate mRNA injections.

βL1221stop mRNAs (~7% and 4% of the currents observed with control oocytes, respectively) (Table 2). For both channels, however, the P_{omax} cGMP was shown to be close to 1 (Table 1), and the possible reduction of unitary current amplitude (Fig. 3) is too small to account for the reduced amplitude of the currents. Very low currents were also obtained with oocytes co-expressing αD608stop and βS1271stop, as well as the shorter β subunit βN1202stop (therefore indicating that the low channel activity is not due to unmasking a retention or degradation sequence that could be present downstream of the nucleotide binding domain in the β subunit). This reduction of activity, which is little-affected by the length of the β subunit, is thus conferred by truncation of the α subunit, although homomeric αD608stop channels have normal activity. αD608stop and β subunits nevertheless assemble with high efficiency; otherwise, large currents with α-only channel characteristics would be expected. It is possible that truncation of the α subunit unmasks a retention or degradation sequence in another part of the β subunit. Another possible explanation could be that, in the absence of the C-terminal domain of the α subunit, channels of different stoichiometries can be formed ($\alpha_3\beta$ or $\alpha\beta_3$), but that they have no channel activity. This question will be addressed elsewhere.

Role of the pore domains

In an attempt to identify other domains that may be responsible for cAMP sensitivity, we constructed two chimeras of α and β subunits: a β subunit with the pore domain of the α subunit (β[α-pore]) and the symmetric construction of the α subunit with the pore domain of the β subunit (α[β-pore]).

Like βwt subunits, β[α-pore] alone had no channel activity. In contrast, when β[α-pore] mRNA was co-injected with αwt mRNA, cGMP-induced currents that could be inhibited by L-*cis*-diltiazem (67% ± 2%) were observed (Table 3), indicating that the channels were at least for a large part heteromeric channels. However, the cAMP sensitivity of these channels was reduced to that of α-only channels, or even lower ($I_{max(cAMP)}/I_{max(cGMP)}$ = 0.024 ± 0.002). Because the sensitivity to cAMP of heteromeric channels containing truncated α and β subunits is markedly increased (see above), we also studied the cAMP sensitivity of heteromeric αD608stop/β[α-pore]L1221stop and αR656/β[α-pore]L1221stop channels to determine which of the two modifications (pore exchange or C-terminal truncation) predominates. For these two types of channels (Table 3), cAMP sensitivity was inferior or equal to that of α-only channels, while L-*cis*-diltiazem sensitivity was unambiguously different from that of α-only channels, and close to that of αD608stop/βL1221stop or αR656/βL1221stop channels, respectively (Table 1), indicating that the channel population was mainly composed of heteromers. The $I_{max(cAMP)}/I_{max(cGMP)}$ measured for heteromeric channels with chimeric β subunits having an α-pore domain are compared in Fig. 7 to those measured with the corresponding channels containing nonchimeric β subunits. These results show that the pore domain of the β subunit plays a key role concerning the gating efficacy of cAMP, and that C-terminal truncation of the α subunit has no effect if the pore of the β subunit is exchanged for that of the α subunit.

No channel activity was detected with the α[β-pore] subunit mRNA, either when injected alone or when co-

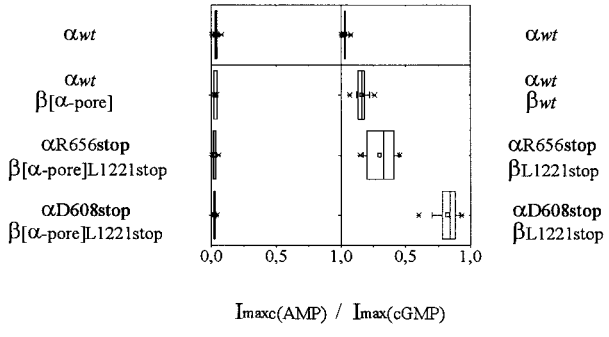

FIGURE 7 Effect of exchanging the pore domain of the β subunit by that of the α subunit on the sensitivity to cAMP of heteromeric channels. Statistical box charts for $I_{max(cAMP)}/I_{max(cGMP)}$ ratios (from macroscopic $I_{max(cAMP)}$ and $I_{max(cGMP)}$ measured on the same patch) obtained for heteromeric channels containing βwt or βL1221stop subunits (right part, same data as in Fig. 6), or the corresponding chimeric β subunits in which the pore domain was exchanged for that of the α subunit (left part). All the channel populations mainly consisted of heteromeric channels, as proved by the extent of inhibition by diltiazem (Tables 2 and 3). The $I_{max(cAMP)}/I_{max(cGMP)}$ ratio of αwt channels is shown for comparison. Mean values are given in Tables 2 and 3. cGMP: 500 μM; cAMP: 20 mM.

injected with αwt mRNA, βwt mRNA, or with $\beta[\alpha$-pore] mRNA.

DISCUSSION

The results presented here demonstrate the role of two domains of the retinal cGMP-activated channel, distinct from the nucleotide-binding site, concerning the sensitivity to cAMP: a conserved C-terminal domain situated downstream of the cGMP-binding site in the α subunit (PD004548), and the pore domain of the β subunit. Exchanging the pore domains or removing the C-terminal domains produces much larger changes in sensitivity than any previously reported mutation.

The pore domain of the β subunit

The possible influence of the pore of the β subunit on the activity of heteromeric channels has not been studied previously. The striking finding presented here (Fig. 7) is that replacing the pore of the β subunit by that of the α subunit completely abolishes the effect of the β subunit on the sensitivity to cAMP of heteromeric channels. Moreover, truncation of the C-terminal domain PD004548 in the α subunit, which increases cAMP sensitivity, has no effect if the pore of the β subunit is exchanged for that of the α subunit: this suggests that high cAMP sensitivity is in fact due to the β-pore domain but is partially masked in the presence of αwt, and that the effect of deleting PD004548 in the α subunit is to relieve this inhibition of cAMP sensitivity rather than to directly increase cAMP sensitivity.

The exchanged domains only comprise 16 residues: the α-pore segment V_{348}YSLYWSTLTLTTIGET$_{364}$ replacing I_{947}RCYYWAVKTLITIGGL$_{963}$ in the β subunit. The main difference between the two pore domains (Fig. 2) is the presence of distinct charged residues. E363 near the selectivity filter of the rod α subunit was shown to be responsible for calcium block of homomeric α channels (Root and MacKinnon, 1993; Eismann et al., 1994). Mutating the corresponding residue in the olfactory neuron α subunit is also responsible for calcium blockage, and decreases the gating efficacy of both cGMP and cAMP (Gavazzo et al., 2000). The residue at the corresponding place in the β subunit is uncharged (G962), and an acid residue is situated three residues downstream (D965) in place of P366 in the α subunit. In addition, there are two basic residues (R948 and K955) in the pore of the β subunit (corresponding to the hydrophobic residues Y349 and L356 in the α subunit). Point mutations of the corresponding residues in the pore of the α subunit will be needed to determine the residue(s) responsible for the effect. It is interesting that the pore of the third olfactory channel subunit (CNG4.3 or CNGβ1b, identical to the rod β subunit: Sautter et al., 1998; Bönigk et al., 1999) and that of the β subunit of the cone channel (human and mouse: Sundin et al., 2000; Kohl et al., 2000; Gerstner et al., 2000), which are also responsible for increased cAMP sensitivity of these channels, contain two basic residues and an acid residue at the same positions as the rod β subunit (Fig. 2). However, although the second olfactory channel subunit (OCNC2) also confers increased cAMP sensitivity to the α subunit (Liman and Buck, 1994; Bradley et al., 1994) its pore does not contain the three charged residues as that of the other β subunits; in fact, for its pore domain, this subunit is homologous to an α subunit.

The fact that the symmetric construct $\alpha[\beta$-pore], expressed alone or with βwt subunits, has no channel activity suggests that four β-pore domains are unable to form a functional cationic channel. However, this is not the only reason for the absence of activity of β subunits alone, because $\beta[\alpha$-pore]s have no channel activity either when expressed alone. The fact that $\alpha[\beta$-pore] has no channel activity when expressed with αwt or $\beta[\alpha$-pore] moreover suggests that the β-pore domain may be unable to function when inserted in the α subunit. Alternatively, the absence of detected activity could be due to rapid inactivation, as previously observed for several mutants of the residue E363 in the pore of the rod α subunit (Bucossi et al., 1996); given our experimental conditions, however, we estimate that inactivation should be complete in $<$10 ms after the start of the voltage pulse to remain undetected.

The C-terminal domains

The other striking finding is the role of the C-terminal domain downstream of the cGMP-binding site of the α subunit in heteromeric channel function. When the α subunit truncated downstream of D608, which corresponds to the deletion of the whole C-terminal domain downstream of the cGMP-binding site, is co-expressed with truncated β subunits, a drastic effect on cAMP sensitivity is observed (P_{omax} cAMP measured from single-channel records and $I_{\mathrm{max(cAMP)}}/I_{\mathrm{max(cGMP)}}$ ratio measured from macroscopic currents: Table 1 and 2). Truncation of the α subunit C-terminus domain downstream of K665 has little effect, while truncation downstream of R656 has a partial but well-marked effect, suggesting that the presence of the entire predicted α-helix of the PD004548 domain downstream of the cGMP-binding site plays a major role for cAMP sensitivity of wild-type heteromeric channels.

The discrepancies between the values obtained from single-channel records and macroscopic current measurements might be explained by the irregular occurrence of long closed periods in cAMP-, and (although to a lesser extent) in cGMP-induced currents (see Fig. 3), which are fully taken into account in macroscopic currents, but poorly in single-channel analysis. The errors on P_{omax} (cAMP) and P_{omax} (cGMP) add up in the P_{omax} (cAMP)/P_{omax} (cGMP) ratio. However, a proportion of α-only channels can be present in the patches from oocytes injected with α and β

mRNAs used for macroscopic current measurements; comparing the values for the extent of inhibition by diltiazem in Table 1 (single-channel) and Table 2 (macroscopic currents) suggests that part of the macroscopic currents in patches from oocytes co-injected with α and β mRNAs is due to homomeric channels.

The EC_{50} for cAMP measured from macroscopic currents of oocytes expressing αD608stop/βL1221stop channels is also very much reduced (224 $\pm$ 6 μM), as is the EC_{50} for cGMP (22 $\pm$ 2 μM) compared to those of $\alpha wt/\beta wt$ channels (1607 $\pm$ 31 μM and 35 $\pm$ 0.6 μM, respectively) (Fig. 5). After normalizing the dose-response curves to the P_{omax} values obtained from single-channel records, the dose-response curves for cAMP and cGMP of the αD608stop/βL1221stop channel were fitted with the MWC allosteric model (Monod et al., 1965) (Fig. 8), which can be used as an approximation of the CNG channel mechanism (Zagotta and Siegelbaum, 1996). According to this model, stabilization of the open state is achieved independently of the ligand by decreasing the parameter L ($L = [T]/[R]$, equilibrium constant between closed and open states in the absence of ligand), which is a characteristic of the protein. The equilibrium constant between fully liganded closed and open states being equal to Lc^4, the open state can be stabilized in the presence of ligand by decreasing L and/or by decreasing $c = K_R/K_T$ (ratio of the affinity of the ligand for the closed state to the affinity for the open state). Fig. 8 shows that it is possible to fit the data by only reducing c and K_R for both ligands (without reducing L), but that decreasing L only cannot account for the data: when L is reduced, whatever its value, it is necessary to also decrease c (increase the gating efficacy) and K_R (increase the affinity of the open state) for cAMP. Thus, interpreting the data with the MWC model suggests that, in αD608stop/βL1221stop channels, the conformation of nucleotide binding sites is different from that of the wild-type channel; i.e., that the C-terminal domains constrain the conformation of the nucleotide binding sites, resulting in lowering the efficacy of cGMP and more particularly, cAMP (increase "c" and "K_R"). The fit does not exclude that the truncation may in addition facilitate the transition to the open state (reduce "L"). It should be noted that although high cAMP sensitivity is conferred by the β subunit (as discussed above), most of the constraint is relieved by truncating the C-terminus of the α subunit (compare dose-response curves for $\alpha wt/\beta$L1221stop and for αD608stop/βL1221stop, Fig. 5), suggesting that intersubunit interactions are involved in the conformation of the oligomer.

Finally, our results indicate that although L-*cis*-diltiazem sensitivity is conferred to the rod channel by the β subunit, the presence of part of the PD004548 domain in the α subunit (D608-R656) is necessary for full inhibition of heteromeric channels. Complete inhibition of heteromeric channels containing truncated βL1221stop subunits (αK665stop/βL1221stop and αR656stop/βL1221stop, Table 1 and Fig. 3) indicates that the C-terminus downstream of L1221 in the β subunit is not involved in L-*cis*-diltiazem sensitivity. The fact that heteromeric channels with a chimeric β subunit having the pore of the α subunit have a sensitivity to diltiazem similar to that of the corresponding heteromers with nonchimeric β subunits (Table 3) indicates that the pore of the β subunits is not involved either.

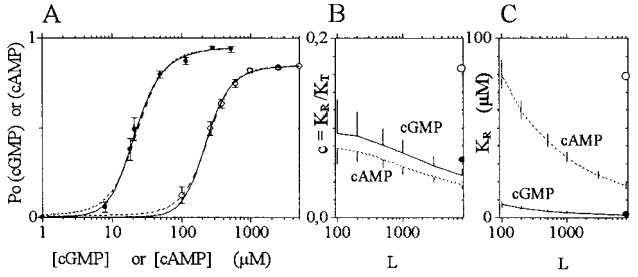

FIGURE 8 Fits of dose-response curves for αD608stop/βL1221stop channels according to the MWC allosteric model (Monod et al., 1965). The data, $\pm$SE, are the same as in Fig. 5, but are expressed in open probabilities; currents are normalized to the value of P_{omax} cGMP (0.93) and P_{omax} cAMP (0.86) from Table 1. The dose-response curves cannot be fitted with a reasonable error with the MWC model without fixing any of the parameters (L, c, K_R). We have fitted the data for varying values of L between $L = 7999$ (measured for αwt, Tibbs et al., 1997) and $L = 100$ (chosen as the lowest value compatible with the absence of detectable spontaneous openings), corresponding to a probability of spontaneous openings $P_{sp} = 1/(L + 1) \sim 0.01$. The fits corresponding to the extreme values are shown in *A*: the solid line corresponds to $L = 7999$ (K_RcGMP = 1.47 $\pm$ 0.17 μM, $c = 0.047 \pm 0.007$; K_RcAMP = 17.6 $\pm$ 1.6 μM, $c = 0.037 \pm 0.005$), and the dashed line corresponds to $L = 100$ (K_RcGMP = 7.4 $\pm$ 1.5 μM, $c = 0.094 \pm 0.04$; K_RcAMP = 80 $\pm$ 8 μM, $c = 0.077 \pm 0.017$). Note that these are only global values, since the simple MWC model does not take into account the existence of two types of sites. The values of c (for cGMP and cAMP) and of K_R (for cGMP and cAMP) that give the best fit for each value of L are plotted in *B* and *C* as a function of L; error bars are shown for several points. The values calculated for $\alpha wt/\beta wt$ channels with $L = 7999$ (Pagès et al., 2000) are indicated on the two plots with solid (cGMP) or open (cAMP) circles: c (cGMP) = 0.065 $\pm$ 0.001, c (cAMP) = 0.166 $\pm$ 0.001, and K_RcGMP = 1.89 $\pm$ 0.04 μM, K_RcAMP = 79 $\pm$ 0.4 μM. The graph in *A* shows that the data can be reasonably fitted with any value of L between 7999 and 100, although the fit with $L = 100$ appears less satisfying at low nucleotide concentrations. *B* and *C* show that it is not possible to fit the cAMP dose-response curve by reducing L only: reducing both K_R(cAMP) and c are also necessary.

As stated in the Introduction, part of PD004548 (which is conserved in rod, olfactory neuron, and cone α subunits) and of PD012882 (which is only conserved in rod β subunits) are predicted as possible coiled-coil forming domains. Although structure predictions should only be considered as speculation, this raises the attractive hypothesis that these domains might constitute oligomerization domains. While the C-terminal domains of the β subunits of the rod, olfactory neuron (OCNC2), and cone have low sequence homology, the domains downstream of the nucleotide binding site in all three β subunits are predicted to have an α-helical structure, suggesting a structural homology between CNG channel β subunits that may be impor-

tant for channel function. The α-helical domain of the OCNC2 subunit is moreover also predicted to form a coiled-coil structure with a high probability, although it is less clear for the cone β subunit. It is interesting that PD004548 in the α subunit, which is best conserved between CNG channels, also has a determinant role, while deletion of PD012882 in the β subunit has less consequence on channel activity. As CNG channels assemble as two dimers with dimerization at the level of the nucleotide binding site (Liu et al., 1998; Shammat and Gordon, 1999; He et al., 2000), it is tempting to speculate that coiled-coil structures could be formed between the domains downstream of the nucleotide binding site of two subunits (either adjacent or diagonally arranged), or of the four subunits, forming a four-helix bundle, as described for the KcsA K^+ channel (Cortes et al., 2001). Such a structure would be likely to constrain the conformation of the protein domains situated upstream or to limit their rotation freedom, and may account for the fact that although high cAMP sensitivity is due the β subunit, deletion of the C-terminal domain of the α subunit relieves most of the constraint. Interaction between C-terminal domains may, in addition, participate in determining the subunit arrangement and favoring the $\alpha_2\beta_2$ stoichiometry.

CONCLUSIONS

The pore domain of the β subunit is potentially able to confer high cAMP sensitivity (EC_{50} and open probability), but this effect is partially masked in the presence of the C-terminal domain of the αwt subunit, and revealed by truncation of the PD004548 domain. Although the effect of C-terminal truncations on cGMP sensitivity (EC_{50}) is less dramatic, it is nevertheless clearly observed for αD608stop/βL1221stop channels, suggesting that it is not specific to cAMP, but is only more visible due to the fact that cAMP, contrary to cGMP, is not able to stabilize the open state on its own. Binding of cAMP can achieve the same result as cGMP only with the additional open-state-stabilizing (activating) effect of the pore of the β subunit, and removal of the closed-state-stabilizing (inhibitory) effect of the C-terminal domains. The facts that PD004548 is highly conserved in all α subunits of the CNG channel family, that some structural homology is predicted for the corresponding domain in β subunits, and that charged residues in the pore domain of the rod channel β subunit are conserved in other β subunits, suggest that these findings may apply to all CNG channels.

Note added in proof

Because the Grenoble vision group has ceased activity due to a reorientation of the scientific scope of the CEA, this work will not be continued.

While this paper was in proof, Trudeau and Zagotta published a study on a similar subject (*Neuron*. 34). This prompts us to add here two related preliminary observations, which would be worth verifying: (1) a $\beta_{572\text{-}766}$-$\alpha_{163\text{-}690}$ chimera (corresponding to the α subunit having the cytoplasmic N-terminal domain of the β subunit), in which the potential retention sequence $R_{626}KR$ in the β subunit was mutated to AAA, had no channel activity; (2) oocytes co-expressing the symmetric $\alpha_{1\text{-}162}$-$\beta_{767\text{-}1393}$ chimera (β subunit having the N-terminal cytoplasmic domain of the α subunit) and αD608stop had low currents, like oocytes co-expressing βwt and αD608stop.

We thank Pr. U.B. Kaupp for the gift of the rod channel α subunit. F.P. was the recipient of a fellowship from the Association Française Retinitis Pigmentosa (AFRP).

REFERENCES

Becchetti, A., K. Gamel, and V. Torre. 1999. Cyclic nucleotide-gated channels: pore topology studied through the accessibility of reporter cysteines. *J. Gen. Physiol.* 114:377–392.

Becchetti, A., and P. Roncaglia. 2000. Cyclic nucleotide-gated channels: intra- and extracellular accessibility to Cd^{2+} of substituted cysteine residues within the P-loop. *Pflugers Arch.* 440:556–565.

Biel, M., X. Zong, A. Ludwig, A. Sautter, and F. Hofmann. 1996. Molecular cloning and expression of a modulatory subunit of the cyclic nucleotide-gated cation channel. *J. Biol. Chem.* 271:6349–6355.

Bönigk, W., J. Bradley, F. Muller, F. Sesti, I. Boekhoff, G. V. Ronnett, U. B. Kaupp, and S. Frings. 1999. The native rat olfactory cyclic nucleotide-gated channel is composed of three distinct subunits. *Neuroscience.* 19:5332–5347.

Bradley, J., J. Li, N. Davidson, H. Lester, and K. Zinn. 1994. Heteromeric olfactory cyclic nucleotide-gated channel: a subunit that confers increased sensitivity to cAMP. *Proc. Natl. Acad. Sci. U.S.A.* 91: 8890–8894.

Bucossi, G., E. Eismann, F. Sesti, M. Nizzari, M. Seri, U. B. Kaupp, and V. Torre. 1996. Time-dependent current decline in cyclic GMP-gated bovine channels caused by point mutations in the pore region expressed in *Xenopus* oocytes. *J. Physiol.* 493:2:409–418.

Chen, T.-Y., Y.-W. Peng, R. S. Dhallan, B. Ahamed, R. R. Reed, and K.-W. Yau. 1993. A new subunit of the cyclic nucleotide-gated cation channel in retinal rod. *Nature.* 362:764–767.

Corpet, F., F. Servant, J. Gouzy, and D. Kahn. 2000. ProDom and ProDom-CG: tools for protein domain analysis and whole genome comparisons (ProDom server: http://protein.toulouse.inra.fr/prodom/doc/prodom.html). *Nucleic Acids Res.* 28:267–269.

Cortes, D. M., L. G. Cuello, and E. Perozo. 2001. Molecular architecture of full-length *KcsA*. Role of cytoplasmic domains in ion permeation and activation gating. *J. Gen. Physiol.* 117:165–180.

Doyle, D. A., J. Morais Cabral, R. A. Pfuetzner, A. Kuo, J. M. Gulbis, S. L. Cohen, B. T. Chait, and R. MacKinnon. 1998. The structure of the potassium channel: molecular basis of K^+ conduction and selectivity. *Science.* 280:69–77.

Eismann, E., F. Muller, S. H. Heinemann, and U. B. Kaupp. 1994. A single negative charge within the pore region of a cGMP-gated channel controls rectification, Ca^{2+} blockage, and ionic selectivity. *Proc. Natl. Acad. Sci. U.S.A.* 91:1109–1113.

Flynn, G. E., and W. N. Zagotta. 2001. Conformational changes in S6 coupled to the opening of cyclic nucleotide-gated channels. *Neuron.* 30:689–698.

Fodor, A. A., and W. N. Zagotta. 1996. Subunit 2 alters ligand specificity of rod CNG channels. *Biophys. J.* 70:368*a*. (Abstr.).

Gavazzo, P., C. Picco, E. Eismann, U. B. Kaupp, and A. Menini. 2000. A point mutation in the pore region alters gating, Ca^{2+} blockage, and permeation of olfactory cyclic nucleotide-gated channels. *J. Gen. Physiol.* 116:311–326.

Gavazzo, P., C. Picco, L. Maxia, and A. Menini. 1996. Properties of native and cloned cyclic nucleotide gated channels from bovine. *In* Neurobiology: Ionic Channels, Neurons, and the Brain. V. Torre and F. Conti, editors. Plenum Press, New-York. 75–83.

Gerstner, A., X. Zong, F. Hofmann, and M. Biel. 2000. Molecular cloning and functional characterization of a new modulatory cyclic nucleotide-gated channel subunit from mouse retina. *J. Neurosci.* 20:1324–1332.

Gordon, S. E., J. C. Oakley, M. D. Varnum, and W. N. Zagotta. 1996. Altered ligand specificity by protonation in the ligand binding domain of cyclic nucleotide-gated channels. *Biochemistry.* 35:3994–4001.

He, Y., M. Ruiz, and J. W. Karpen. 2000. Constraining the subunit order of rod cyclic nucleotide-gated channels reveals a diagonal arrangement of like subunits. *Proc. Natl. Acad. Sci. U.S.A.* 97:895–900.

Johnson, J. P., and W. N. Zagotta. 2001. Rotational movement during cyclic nucleotide-gated channel opening. *Nature.* 412:917–921.

Kaupp, U. B., T. Niidome, T. Tanabe, S. Terada, W. Bönigk, W. Stühmer, N. Cook, K. Kangawa, H. Matsuo, T. Hirose, T. Miyata, and S. Numa. 1989. Primary structure and functional expression from complementary cDNA of the rod cGMP-gated channel. *Nature.* 342:762–766.

Kohl, S., B. Baumann, M. Broghammer, H. Jagle, P. Sieving, U. Kellner, R. Spegal, M. Anastasi, E. Zrenner, L. T. Sharpe, and B. Wissinger. 2000. Mutations in the CNGB3 gene encoding the beta-subunit of the cone photoreceptor cGMP-gated channel are responsible for achromatopsia (ACHM3) linked to chromosome 8q21. *Hum. Mol. Genet.* 9:2107–2116.

Körschen, H. G., M. Illing, R. Seifert, F. Sesti, A. Williams, S. Gotzes, C. Colville, F. Müller, A. Dose, M. Godde, L. Molday, U. B. Kaupp, and R. S. Molday. 1995. A 240 kDa protein represents the complete β subunit of the cGMP-gated channel from rod photoreceptor. *Neuron.* 15:627–636.

Kozak, M. 1984. Compilation and analysis of sequences upstream from the translational start site in eukaryotic mRNAs. *Nucleic Acids Res.* 12: 857–872.

Kumar, V. D., and I. T. Weber. 1992. Molecular model of the cyclic GMP-binding domain of the cyclic GMP-gated ion channel. *Biochemistry.* 31:4643–4649.

Liman, E. R., and L. B. Buck. 1994. A second subunit of the olfactory cyclic nucleotide-gated channel confers high sensitivity to cAMP. *Neuron.* 13:611–621.

Liman, E. R., J. Tytgat, and P. Hess. 1992. Subunit stoichiometry of a mammalian K^+ channel determined by construction of multimeric cDNAs. *Neuron.* 9:861–871.

Liu, J., and S. A. Siegelbaum. 2000. Change of pore helix conformational state upon opening of cyclic nucleotide-gated channels. *Neuron.* 28: 899–909.

Liu, D. T., G. R. Tibbs, P. Paoletti, and S. A. Siegelbaum. 1998. Constraining ligand-binding site stoichiometry suggests that a cyclic-nucleotide gated channel is composed of two functional dimers. *Neuron.* 21:235–248.

Liu, D. T., G. R. Tibbs, and S. A. Siegelbaum. 1996. Subunit stoichiometry of cyclic nucleotide-gated channels and effects of subunit order on channel function. *Neuron.* 16:983–990.

Lupas, A. 1996. Prediction and analysis of coiled-coil structures (COILS server: http://www.ch.embnet.org/software/COILS form.html). *Methods Enzymol.* 266:513–525.

Monod, J., J. Wyman, and J. P. Changeux. 1965. On the nature of allosteric transitions: a plausible model. *J. Mol. Biol.* 12:88–118.

Pagès, F., M. Ildefonse, M. Ragno, S. Crouzy, and N. Bennett. 2000. Coexpression of α and β subunits of the rod cyclic GMP-gated channel restores native sensitivity to cyclic AMP: role of D604/N1201. *Biophys. J.* 78:1227–1239.

Passner, J. M., S. C. Schultz, and T. A. Steitz. 2000. Modeling the cAMP-induced allosteric transition using the crystal structure of CAP-cAMP at 2.1 Å resolution. *J. Mol. Biol.* 304:847–859.

Perozo, E., D. M. Cortes, and L. G. Cuello. 1999. Structural rearrangements underlying K^+-channel activation gating. *Science.* 285:73–78.

Picco, C., C. Sanfilippo, P. Gavazzo, and A. Menini. 1996. Modulation by internal protons of native cyclic nucleotide-gated channels from retinal rods. *J. Gen. Physiol.* 108:265–276.

Root, M. J., and R. MacKinnon. 1993. Identification of an external divalent cation-binding site in the pore of a cGMP-activated channel. *Neuron.* 11:459–466.

Rost, B., and C. Sander. 1993. Prediction of protein secondary structure at better than 70% accuracy. (The PredictProtein server: http://dodo.cpmc.columbia.edu/predictprotein/). *J. Mol. Biol.* 232:584–599.

Rubin, M. M., and J. P. Changeux. 1966. On the nature of the allosteric transition: implications of non-exclusive ligand binding. *J. Mol. Biol.* 21:265–274.

Sautter, A., X. Zong, F. Hofmann, and M. Biel. 1998. An isoform of the rod photoreceptor cyclic nucleotide-gated channel β subunit expressed in olfactory neurons. *Proc. Natl. Acad. Sci. U.S.A.* 95:4696–4701.

Shabb, J. B., and J. D. Corbin. 1992. Cyclic nucleotide-binding domains in proteins having diverse functions. *J. Biol. Chem.* 267:5723–5726.

Shammat, I. M., and S. E. Gordon. 1999. Stoichiometry and arrangement of subunits in rod cyclic nucleotide-gated channels. *Neuron.* 23: 809–819.

Sundin, O. H., J. M. Yang, Y. Li, D. Zhu, J. N. Hurd, T. N. Mitchell, E. D. Silva, and I. H. Maumenee. 2000. Genetic basis of total colour-blindness among the pingelapese islanders. *Nat. Genet.* 25:289–293.

Tanaka, J. C., J. F. Eccleston, and R. E. Furman. 1989. Photoreceptor channel activation by nucleotide derivatives. *Biochemistry.* 28: 2776–2784.

Tibbs, G. R., E. H. Goulding, and S. A. Siegelbaum. 1997. Allosteric activation and tuning of ligand efficacy in cyclic nucleotide-gated channels. *Nature.* 386:612–615.

Zagotta, W. N., and S. A. Siegelbaum. 1996. Structure and function of cyclic nucleotide-gated channels. *Annu. Rev. Neurosci.* 19:235–263.